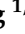



Article

Diurnal Variation Reveals the Characteristics and Influencing Factors of Cool Island Effects in Urban Blue-Green Spaces

Ruixue Kong^{1,2}, Yaqi Chu^{3,*}, Yuanman Hu^{2,4}, Huanxue Zhang¹ , Qiuyue Wang^{2,5} and Chunlin Li^{2,4,*} 

¹ College of Geography and Environment, Shandong Normal University, Jinan 250300, China; kongruixuexue@163.com (R.K.); zhanghuanxue@sdu.edu.cn (H.Z.)

² CAS Key Laboratory of Forest Ecology and Silviculture, Institute of Applied Ecology, Chinese Academy of Sciences, Shenyang 110016, China; huym@iae.ac.cn (Y.H.); w1663924723@163.com (Q.W.)

³ College of Architecture and Engineering, Shenyang University, Shenyang 110044, China

⁴ E'erguna Wetland Ecosystem Research Station, Hulunbuir 022250, China

⁵ College of Resources and Environment, University of Chinese Academy of Sciences, Beijing 101408, China

* Correspondence: chuyaqi@syu.edu.cn (Y.C.); lichunlin@iae.ac.cn (C.L.)

Abstract: Urban blue-green space cooling island effect (BGCI) is effective in improving the thermal comfort of residents. However, there is little knowledge regarding the diurnal variation of BGCI and the influencing factors. Therefore, we selected Beijing as the study area and used ECOSTRESS LST data and the inflection–maximum perspective method to explore the diurnal variation of BGCI. Additionally, we investigated diurnal variations in the relative influence of the characteristics of the blue-green space itself, as well as the surrounding 2D and 3D landscape metrics using boosted regression tree model. The results indicated that BGCI displayed distinct diurnal patterns. BGCI progressively increased from sunrise to midday, decreased thereafter to sunset, reached its peak around midday, and diminished to a relatively low level and constant intensity at night. BGCI of water bodies exhibited a significantly higher intensity compared to vegetation during the day, particularly around midday, with a difference in mean cooling intensity (CI) of 1.06 °C and mean cooling distance (CD) of 63.27 m, while the differences were minimal at night with a difference in mean CI of 0.02 °C and mean CD of 9.64 m. The features of vegetation had a more significant impact on BGCI during the day, particularly around midday (CI: 32.30% around midday and 13.86% at night), while the 3D metrics influenced BGCI more at night (CI: 26.40% around midday and 35.81% at night). The features of water bodies had a greater impact during the midday (52.87% around midday and 10.46% at night), with the landscape metrics of surrounding water bodies playing a more important role at night (15.56% around midday and 38.28% at night). The effect of tree height, shape index of vegetation, and surrounding building coverage ratio of water bodies on BGCI exhibited opposite trends around midday and at night. Optimizing the landscape surrounding blue-green spaces is more cost-effective than the blue-green spaces themselves for nighttime thermal comfort, especially in 3D urban landscapes. These findings emphasize the imperative and essentiality of exploring diurnal variations in BGCI, providing valuable information for mitigating UHI effects.

Keywords: cool islands; blue-green spaces; urban landscape metrics; diurnal variations; UHI



Citation: Kong, R.; Chu, Y.; Hu, Y.; Zhang, H.; Wang, Q.; Li, C. Diurnal Variation Reveals the Characteristics and Influencing Factors of Cool Island Effects in Urban Blue-Green Spaces.

Forests **2024**, *15*, 2115.

<https://doi.org/10.3390/f15122115>

15122115

Academic Editor: Zhibin Ren

Received: 31 October 2024

Revised: 25 November 2024

Accepted: 27 November 2024

Published: 29 November 2024



Copyright: © 2024 by the authors. Licensee MDPI, Basel, Switzerland. This article is an open access article distributed under the terms and conditions of the Creative Commons Attribution (CC BY) license (<https://creativecommons.org/licenses/by/4.0/>).

1. Introduction

Under the dual impacts of persistent climate change and urbanization, the urban heat island (UHI) effect [1] will further exacerbate extreme precipitation [2,3] and air pollution [4,5], increase energy consumption [6,7], raise heat stress risks [8,9], increase risks of infectious diseases and allergic reactions [10,11], and even contribute to increased mortality rates [12,13]. These impacts significantly inconvenience the lives of urban residents, who make up more than half of the world's population [14,15]. Additionally, both daytime and nighttime UHI patches are expanding [16]. Nocturnal heatwaves have a dramatic

impact on human health and energy consumption [17]. Mortality due to heat at night is expected to be higher than that due to average daily temperatures [18,19]. There is a discernible increase in the intensity, frequency, and duration of nighttime heatwaves and heat stress [20,21]. Therefore, it is urgent to alleviate UHI both during the daytime and nighttime.

Researchers have found that urban blue-green spaces represent the most cost-effective, environmentally friendly, and politically acceptable strategies for mitigating UHI [22–24]. The land surface temperature (LST) of urban blue-green spaces is observed to be lower than that of the surrounding areas, a phenomenon known as the urban blue-green space “cooling islands effect” (BGCI) [25,26]. Nevertheless, the unrestricted expansion of urban blue-green spaces is not feasible due to the lack of available urban land resources and the associated costs of management [27]. Therefore, investigating the BGCI, along with their spatiotemporal patterns, heterogeneity, and influencing factors, holds significant meaning for cost-effectively mitigating UHI and enhancing thermal comfort for urban residents. In addition, previous studies have shown that water bodies exhibit a stronger cold island effect compared to vegetation [28]. However, most of these studies have only focused on the differences between vegetation and water bodies during the daytime, with a lack of research on the nighttime and diurnal variations of BGCI and differences [29]. Currently, there have been a few studies conducted on the nighttime and diurnal variations of BGCI using field measurements and numerical modeling [30–33]. It has been found that nighttime BGCI can also enhance urban thermal comfort. For example, urban vegetation in London can cool up to 440 m, reducing air temperatures by up to 4 °C at night [34]. The simulations show that at night, canopy and grass areas are linearly and positively correlated with cooling distance and nonlinearly with cooling intensity [35]. Qian et al. (2024) found that both vegetation and water bodies exhibited diurnal variations in their effects on the 3D thermal environment via UAVs [36].

Field measurements can only study a small number of blue-green spaces, and numerical modeling is lacking in the study of complex cities [37]. The application of remote sensing technology represents a promising avenue for addressing these challenges [38]. However, few remote sensing techniques have been used to study the diurnal variation of BGCI and the differences in diurnal variation between vegetation and water bodies. To comprehensively explore the diurnal variation of BGCI through remote sensing methods, it is necessary to use LST data characterized by both high temporal and spatial resolutions. However, conventional sources of LST data have been inadequate for this purpose. For instance, Landsat LST data are limited by a fixed observation time within each area. Similarly, ASTER LST data, while possessing a spatial resolution of 90 m, suffer from a lack of images available for individual urban centers [39]. Although widely used, MODIS LST data have a spatial resolution of only 1 km and offer merely two fixed-time observations per day per location, limiting the temporal variability captured for a day. Furthermore, while some LST data are provided on an hourly scale, this often results in a compromise of spatial detail. For instance, platforms such as GOES-R, MSG, and FY provide a resolution of 2–5 km. Addressing these limitations, the ECOSTRESS launched in June 2018 stands out as a pivotal advancement. Providing LST data at a spatial resolution of 70 m, with variable observation times and temporal repetition cycles of 3–5 days, ECOSTRESS greatly enhances our capacity to understand diurnal variations of BGCI within urban areas [40,41]. Therefore, ECOSTRESS was selected for this study to explore the diurnal variation of BGCI.

A multitude of factors at the urban landscape scale exert influence on BGCI [42–44]. Previous research has highlighted that the area of urban blue-green spaces plays a predominant role in determining BGCI effect [45], which has a nonlinear positive correlation with BGCI [46–49]. Nevertheless, in constrained regions, blue-green spaces may fail to generate BGCI effect [50] and could even potentially exacerbate the UHI [51]. Chen et al. (2012) observed that when the vegetation area of a park was less than approximately 1 ha, it might not trigger a BGCI effect on the surrounding environment [52]. Meanwhile,

the shape of blue-green spaces and urban land use influence BGCI [53,54]. Furthermore, it has been found that 2D urban landscape indicators surrounding blue-green spaces could also significantly impact BGCI [55,56]. For instance, Du et al. (2022) discovered that parks that interact with their surroundings had a broader cooling range [57]. Liu et al. (2023) and Yang et al. (2024) found that the presence of a water body in the surroundings would have an enhanced effect on the cooling effect [58,59]. Han et al. (2023) found that indicators of surrounding vegetation were essential indicators of the cooling efficiency of parks [60]. Additionally, investigations have demonstrated that 3D urban landscape metrics, including building height, tree height, building volume, sky view factor, etc., also play a significant role in shaping the urban thermal environment [61–64]. Zhang et al. (2022) discovered significant correlations between building density and floor area ratio around vegetation and BGCI [65]. Han et al. (2023) observed substantial influences of surrounding 2D and 3D landscapes on the BGCI of the park, noting nonlinear relationships between primary surrounding landscape indicators and cooling efficiency [60]. Jia et al. (2024) found that building height and vegetation volume had the most significant effect on ambient temperature change [66]. Li et al. (2024) found that in relation to the BGCI of vegetation, building density and floor area ratio are negatively correlated, while the average building height and the standard deviation of building height are positively correlated [67]. However, similar to studies on BGCI, most of the previous studies on influencing factors have focused on a single point in time during the day. There have been no studies on diurnal variations in the contribution of 2D and 3D landscapes.

In this study, the diurnal variation and influencing factors of BGCI in blue-green spaces within the urban area of Beijing were analyzed based on the ECOSTRESS LST data and boosted regression tree (BRT) model. The aims were (1) to investigate the patterns and differences of diurnal variation in cooling islands of urban vegetation and water bodies using the inflection point–maximum perspective method; (2) to analyze the diurnal variation of the relative influences of the characteristics of the blue-green space itself and the surrounding 2D and 3D urban landscape metrics on BGCI; and (3) to analyze changes in the marginal effects of key landscape indicators over the course of a day. This study tries to comprehensively analyze the diurnal variations and influencing factors of the BGCI of blue-green spaces, providing valuable references for mitigating the urban thermal environment by optimizing urban blue-green spaces at the city scale.

2. Materials and Methods

2.1. Study Area

This study focuses on the area within the Fifth Ring Road (116.2°–116.5° E, 39.7°–40.0° N) of Beijing (Figure 1), which encompasses approximately 666 km², with elevations primarily between 30 and 65 m. As one of China's megacities, Beijing has a particularly high level of urbanization, especially within the Fifth Ring Road, which stands as one of the most densely populated and urbanized regions. In addition, the UHI within this area is pronounced [68,69]. Notably, government efforts have led to the creation of numerous blue-green spaces within this region. Beijing is not only representative of compact cities currently, but it may also provide insight into future trends in the development of smaller cities. Therefore, studying the BGCI in compact cities like Beijing holds significant implications for mitigating the UHI and facilitating accurate urban planning and management [59].

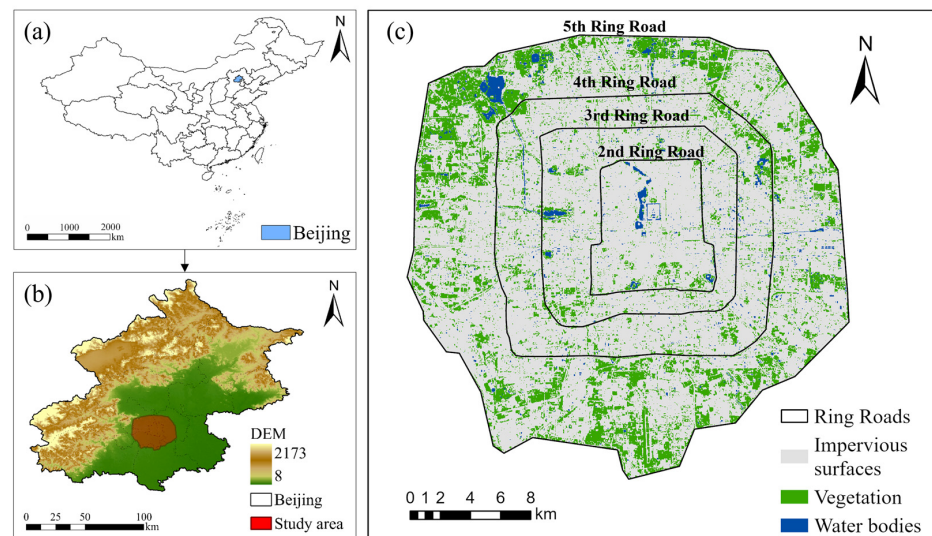


Figure 1. The geographic location of the study area. (a) The location of Beijing within China. (b) The elevations within the administrative boundaries of Beijing and the extent of the study area in Beijing. (c) The land use map of the study area.

2.2. Datasets and Pre-Processing

2.2.1. LST Data

The ECOSTRESS Level 2 product ECO2LSTE (NASA-LPDAAC, <https://lpdaac.usgs.gov/> (accessed on 15 March 2023)) was used to investigate the variation of the BGCI at different times throughout the day and night. Compared to other LST data, this dataset not only offers a higher spatial resolution but also provides a flexible temporal resolution, enabling for the acquisition of data at various time intervals. This dataset provides LST data with a spatial resolution of 70 m and derives LST values from five thermal infrared (TIR) bands ranging from 8 to 12.5 μm , using the physically based Temperature Emissivity Separation (TES) method [40]. This product demonstrated a consistent and reliable performance, with a root mean square error of 1.07 K, a mean absolute error of 0.40 K, and an $R^2 > 0.988$ [41]. Furthermore, this study conducted de-clouding and geo-correction processes using cloud mask products and geolocation products (ECO2CLOUD, ECO1BGEO, <https://lpdaac.usgs.gov/> (accessed on 16 March 2023)). This study selected 9 images under clear atmospheric conditions (few clouds) from June to September 2020 (the hottest months of the year with stable green cover). Table 1 presents the ECOSTRESS acquisition time, LST-related information, and meteorological conditions of the ECOSTRESS images. The meteorological data (<https://rp5.ru/> (accessed on 22 March 2023)) were obtained from the weather station of Beijing (Station ID 54511). In this study, the time 22:32 represents the first half of the night, while the times 01:19, 02:37, and 04:11 represent the second half of the night. Together, these times make up the night. The time 07:20 represents the sunrise, while 10:42, 13:49, and 14:13 represent the time around midday. The time 18:45 represents the sunset, and these times collectively form the day.

Table 1. Related information of ECOSTRESS images.

ECOSTRESS Acquisition Time (Beijing Time)	LST Range	Average LST	Atmospheric Temperature ($^{\circ}\text{C}$)	Relative Humidity (%)	Wind Direction	Wind Speed (m/s)
01:19 on 04 September	10.0–22.7 $^{\circ}\text{C}$	17.0 $^{\circ}\text{C}$	17.2 $^{\circ}\text{C}$	79%	North–northeast	Soft wind (1 m/s)
02:37 on 19 July	8.5–24.9 $^{\circ}\text{C}$	20.2 $^{\circ}\text{C}$	22.3 $^{\circ}\text{C}$	90%	Northeastern	Soft wind (1 m/s)
04:11 on 15 July	18.1–26.2 $^{\circ}\text{C}$	21.7 $^{\circ}\text{C}$	22.3 $^{\circ}\text{C}$	92%	Windless	Windless
07:20 on 07 July	19.7–30.9 $^{\circ}\text{C}$	24.4 $^{\circ}\text{C}$	26.5 $^{\circ}\text{C}$	56%	North	Light wind (3 m/s)
10:42 on 11 August	28.5–51.1 $^{\circ}\text{C}$	38.5 $^{\circ}\text{C}$	31.8 $^{\circ}\text{C}$	49%	North	Light wind (2 m/s)
13:49 on 03 August	27.4–59.5 $^{\circ}\text{C}$	45.2 $^{\circ}\text{C}$	36.5 $^{\circ}\text{C}$	35%	West–southwest	Light wind (2 m/s)
14:13 on 02 June	24.9–52.0 $^{\circ}\text{C}$	40.4 $^{\circ}\text{C}$	31.2 $^{\circ}\text{C}$	32%	South	Light wind (3 m/s)
18:45 on 07 August	15.5–35.3 $^{\circ}\text{C}$	28.1 $^{\circ}\text{C}$	29.9 $^{\circ}\text{C}$	51%	East–southeast	Light wind (2 m/s)
22:32 on 27 September	10.4–20.5 $^{\circ}\text{C}$	16.83 $^{\circ}\text{C}$	20.2 $^{\circ}\text{C}$	72%	South	Light wind (2 m/s)

2.2.2. Blue-Green Spaces and Land Cover Data

Landsat images from 2020 were used to classify land use in the study area on the Google Earth Engine (GEE, <https://earthengine.google.com/> (accessed on 14 April 2023)) platform in this study. Specifically, the Normalized Difference Vegetation Index (NDVI) for the annual maximum and the Modified Normalized Difference Water Index (MNDWI) for the annual mean were initially computed. Subsequently, a triple moving average method was used to reconstruct the NDVI and MNDWI data, aiming to mitigate noise interference [70]. Lastly, the threshold classification method was applied to extract the blue-green spaces (the NDVI and MNDWI thresholds were 0.45 and 0.25, respectively) [71,72]. The overall classification accuracy of 86.05% was assessed based on high-spatial-resolution Google Earth images [73]. The study area was delineated into three categories: impervious surfaces (ISs), vegetation, and water bodies (Figure 1). These land use types were used to calculate the 2D urban landscape metrics. Furthermore, our analysis exclusively focused on blue-green spaces exceeding 1 ha in area, as small blue-green spaces were found to have minimal influences on BGCI [74]. A total of 1399 vegetation patches and 155 water bodies patches were obtained.

2.2.3. Other Data

The building data were obtained from the Polygonal Features of Single Buildings dataset (<https://map.baidu.com> (accessed 1 April 2023)), which includes the footprint of each building and its height. The building footprint in this dataset aligns accurately with the actual buildings, with a total deviation of 1.02 m and an accuracy of 86.78% [75]. Tree height data for this study were extracted from the 2019 Global Forest Canopy Height (GFCH, <https://glad.umd.edu/dataset/gedi/> (accessed 3 April 2023)) at a 30 m spatial resolution, with an RMSE of 9.07 m and R^2 of 0.61 based on available airborne LiDAR data [76]. Furthermore, the 2020 population distribution data were obtained from World Pop (<https://hub.worldpop.org/> (accessed 4 April 2023)). These data have a resolution of 3 arcs (equivalent to 100 m at the equator) and were derived from the 2020 census/projected estimates based on 2020, using output from the Built Settlement Growth Model (BSGM) developed by Jeremiah J. Nieves et al. [77].

2.3. Methods

2.3.1. Quantifying the BGCI Effect

Previous research has demonstrated that the inflection point–maximum perspective method is currently one of the most effective ways to quantify the BGCI effect [78,79]. However, different BGCI indicators suggest varying degrees of significance, and using only one indicator is not comprehensive enough to quantify BGCI. Therefore, this study calculates five BGCI indicators: cooling distance (CD), cooling intensity (CI), cooling rate (CR), cooling efficiency (CE), and cooling service (CS). All five indicators are important for reflecting the influence of vegetation and water bodies on the urban microclimate. Subsequently, to assess the BGCI more comprehensively, the comprehensive cooling effect (CCE) index of blue-green spaces was proposed based on these five normalized BGCI indicators.

Taking into consideration the Landsat spatial resolution of 30 m and drawing on previous related studies [48,80], this study created 20 buffer zones starting from the edge of each blue-green space at fixed intervals of 30 m. We then extracted the average LST of each buffer zone. A polynomial was fitted to the LST–distance plot, and the first-order derivative was used to identify the curve's first turning point in the rising process (Figure 2). The horizontal coordinate of this turning point indicates the furthest distance that the BGCI can reach in the blue-green spaces, referred to as the cooling distance in the blue-green spaces. The detailed calculations and description of BGCI indicators can be found in Table 2.

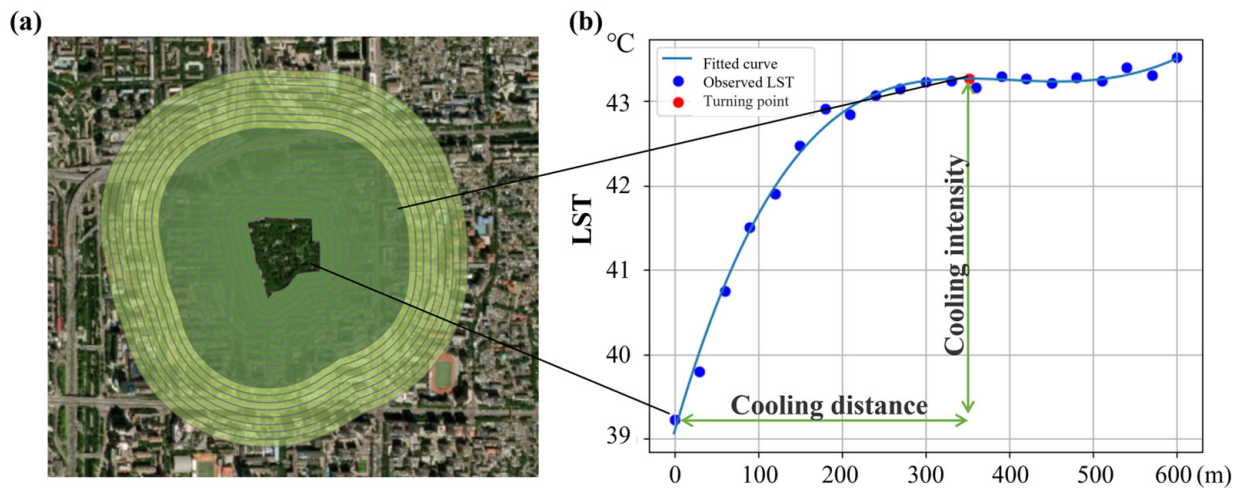


Figure 2. The schematic diagram for calculating BGCI. (a) The buffer zone of vegetation, with dark green representing the maximum cooling range. (b) The LST–distance fitting curve.

Table 2. The formula and description of the BGCI indicators used in the study.

BGCI Indicator	Abbreviation	Formula	Description
Cooling distance	CD	$CD = d$	The furthest distance that BGCI can reach; unit: m.
Cooling intensity	CI	$CI = \Delta T = T_d - T_0$	The maximum LST reduction that can be achieved; unit: °C.
Cooling rate/gradient	CR	$CR = \frac{\Delta T}{d}$	Used to indicate the speed of cooling; unit: °C/m.
Cooling efficiency	CE	$CE = \frac{BGCA}{BGA}$	The area of cooling per unit area of blue-green space. It indicates whether BGCI are economical and effective; unit: none.
Cooling service	CS	$CS = BGCA * \Delta T$	The maximum service degree of BGCI; unit: °C ha.
Comprehensive cooling effect	CCE	$CCE = \frac{CD_n + CI_n + CR_n + CE_n + CS_n}{5}$	An indicator to quantify BGCI in an integrated manner; unit: none.

d represents the furthest cooling distance; *T_d* represents the LST of the furthest cooling distance; *T₀* represents the average LST of the blue-green space; *BGCA* represents the cooling area of blue-green space, i.e., the total area of the buffer within the cooling distance; *BGA* represents the area of the blue-green space; *CD_n*, *CI_n*, *CR_n*, *CE_n*, and *CS_n* represent normalized CD, CI, CR, CE, and CS, respectively.

2.3.2. Calculation of 2D and 3D Landscape Metrics

In this study, 16 landscape indicators were selected to comprehensively quantify the 2D and 3D urban landscape of the study area. In addition, anthropogenic factors (expressed as population in this paper) also affect the urban thermal environment [81,82]. The indicators are categorized into six categories: the 2D features of the blue-green spaces inherent (Feature), the 2D landscape metrics of the surrounding water body (Sur_WAT), the 2D landscape metrics of the surrounding vegetation (Sur_VEG), the 2D landscape metrics of the surrounding impervious surfaces (Sur_ISs), the distribution of the surrounding population (Sur_PEP), and 3D landscape features (3D metrics). The surrounding landscape refers to the buffer zone area within the cooling distance. The 2D feature metrics of blue-green spaces included patch area (AREA) and shape index (LSI). The surrounding landscape (water bodies, vegetation, and ISs) metrics included the proportion of landscape patch area (PLAND), shape index (LSI), spatial aggregation index (AI), proportion of landscape area occupied by the largest patch (LPI), patch connectivity index (NECT), edge density (ED), number of patches (NP), and patch density (PD). For example, the aggregation index of surrounding water bodies is abbreviated as Sur_WAT_AI. The 2D landscape metrics were calculated on a 1 × 1 km grid to provide a comprehensive description of the surrounding 2D urban landscape from multiple perspectives: quantitative, features, spatial agglomeration, and spatial connectivity. The 3D urban metrics, including tree height (TH), building coverage ratio (BCR), building height (BH), building volume (BV), architecture height standard deviation (AHSD), and floor area ratio (FAR), not only quantify the urban landscape but also indirectly reflect human activities around the blue-green spaces. Table 3

presents detailed information on these metrics. This study does not consider the impact of water velocity and elevation metrics on BGCI due to the scarcity of rivers in the study area and the absence of elevation changes. Meanwhile, this study does not take wind direction and speed into consideration as the wind speed is small, ranging from 0 to 3 m/s.

Table 3. Descriptions of 2D and 3D urban landscape metrics in the study.

Types	Subcategory	Indicator	Abbreviations	Descriptions
2D	Feature	Patch area	AREA	The area of the patch; unit: ha.
		Landscape shape index	LSI	Assessing the complexity of the shape of vegetation or water bodies; unit: none.
	Sur_ISs	Percent of landscape	PLAND	The proportion of area occupied by various land types; unit: %.
		Landscape shape index	LSI	Assessing the complexity of the shape of certain types of patches; unit: none.
		Largest path index	LPI	The ratio of the maximum patch area to landscape area, to determine the dominant patch type in the landscape; unit: %.
		Edge density	ED	The ratio of the sum of the lengths of all edge segments of a given type of patch to the area of the landscape, assessing the density of edges in the landscape; unit: m/ha.
		Aggregation index	AI	To assess the degree of aggregation of different types of patches in the landscape, in terms of distance, number, and area of neighboring patches of the same type; unit: none.
		Connectance Index	NECT	To assess the degree of connectivity between patches, reflecting the spatial connectivity between patches of the same land category; unit: none.
		Number of patches	NP	The number of landscape patches in each category; unit: pcs.
		Patch density	PD	The density of patches of a given land category in the landscape. It reflects the degree of fragmentation; unit: #/100 ha.
	Sur_VEG	Same as Sur_ISs		
	Sur_WAT	Same as Sur_ISs		
	Sur_PEP	Population	PEP	The number of populations.
3D	3D metrics	Building coverage ratio	BCR	The extent of building coverage in the study area can be calculated as the ratio of the roof area of the building to the total statistical area; unit: %.
		Building height	BH	The height of buildings; unit: m.
		Building volume	BV	The volume of buildings; unit: m ³ .
		Floor area ratio	FAR	The ratio of the sum of the gross floor area to the statistical unit area. It reflects the extent to which the building is utilized on the statistical unit area; unit: %.
		Architecture height standard	AHSD	The extent of change in building heights in the region; unit: m.
		Tree height	TH	The tree height of the vegetation; unit: m.
		Tree height of the surrounding area	Sur_TH	The tree height of surroundings; unit: m.

2.3.3. Statistical Analysis Methods

Kruskal–Wallis analysis, multiple stepwise regression, and BRT model were combined to analyze the diurnal variations, the relative influences, and the marginal effects of BGCI. Kruskal–Wallis analysis was used to analyze the diurnal variations in the BGCI and to reveal the differences in the BGCI of vegetation and water bodies at different time points by testing whether multiple groups of samples at different time points come from the same distribution. Multiple stepwise regression analysis was used to obtain the combined explanatory rate of the variables entering the model. The BRT model was used to analyze the relative importance and marginal effect of 2D and 3D urban landscape metrics on BGCI at different time points. The BRT combines the strengths of regression trees and enhancement algorithms to estimate the single best predictor variable. Unlike traditional

linear regression models that use regression coefficients to analyze the degree of influence, the BRT model allows for the construction of multiple regression trees to predict the complex nonlinear relationship between independent and dependent variables. The BRT visualizes the marginal effect curve of the dependent variable in relation to a specific independent variable. This visualization helps analyze the correlation of the respective variable with the dependent variable and identify the threshold point of its influential effect. The BRT model uses recursive binary splitting to eliminate interactions between influencing factors and can be used without considering interactions between independent variables [83,84]. BRT outperforms Random Forests and Support Vector Machines in handling data with complex nonlinear relationships and has been widely used in urban thermal environments [61].

3. Results

3.1. Diurnal Variation Characteristics of BGCI

The spatial distribution of CCE in blue-green spaces in the study area was not uniform (Figure 3). The CCE between the Fourth and Fifth Ring Roads was consistently higher than that of other areas throughout the day. Among them, during the day and the first half of the night, the CCE in the northwest between the Fourth and Fifth Ring Roads was consistently relatively high. Furthermore, at night, the CCE in this region continued to decrease until 04:11, when it reached its lowest point. Additionally, at 04:11, the spatial heterogeneity of CCE was at its minimum in the entire study area.

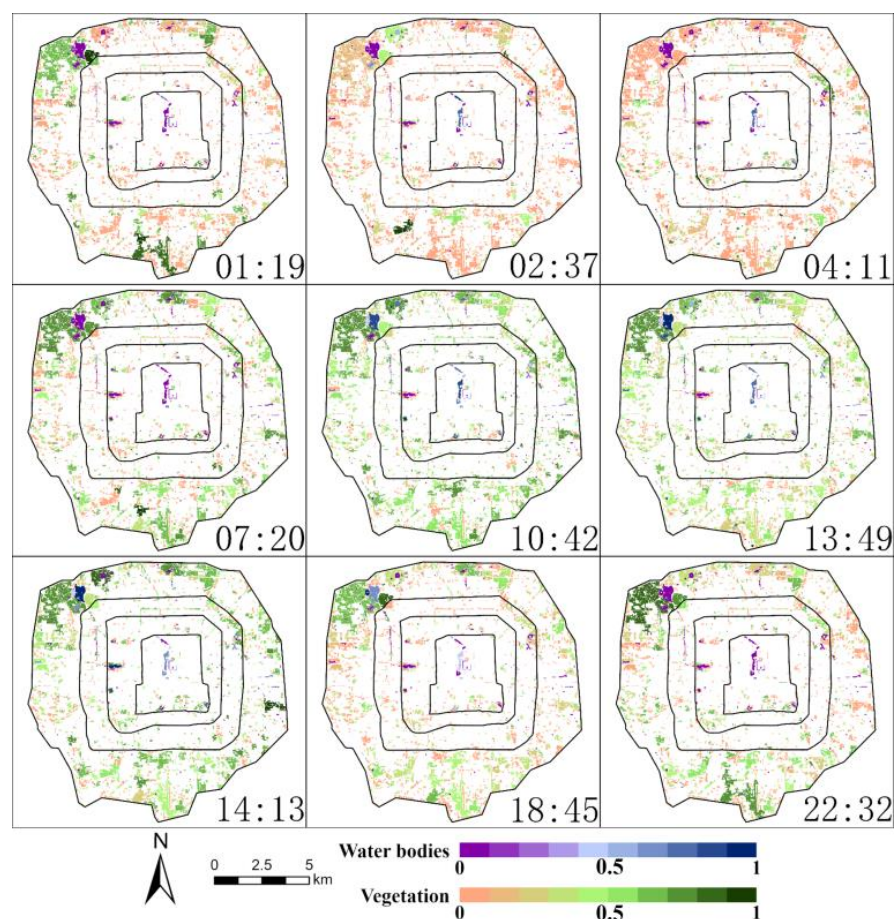


Figure 3. Spatial distribution of comprehensive cooling effect (CCE) at different time points.

BGCI exhibited a distinct pattern of diurnal variations (Figure 4). From sunrise to midday, BGCI continued to rise and peaked around midday, then declined until sunset, with relatively low and insignificant changes at night. In addition, there is little change in the BGCI around midday. The CI, CR, and CS values exhibited similar characteris-

tics (Figure 4b,c,e), with the values being significantly larger around midday than at night and at sunrise, with sunset occurring in the middle, showing a clear day–night difference. For example, the average CI of vegetation was 0.33 °C at sunrise, 1.48 °C around midday, 0.75 °C at sunset, and 0.31 °C at night. Among them, the average CI at 13:49 was the highest (1.78 °C), reaching up to about 20.54 °C. This was followed by 10:42 (1.46 °C) and 14:13 (1.21 °C). The maximum reached 1.93 °C during the night. For water bodies, it was 0.24 °C, 2.54 °C, 1.05 °C, and 0.33 °C, respectively. Among them, the average CI at 13:49 was the highest (2.81 °C), reaching up to about 8.42 °C. This was followed by 14:13 (2.39 °C) and 10:42 (2.15 °C). The mean CI difference between the time points around noon was 0.5 °C. It reached a maximum of 2.25 °C during the night. However, CD, CE, and CCE were similar (Figure 4a,d,f), and although they are all larger around midday than at night, there is little difference in the values at each time point relative to the other three indicators. For example, the average CD of vegetation was 239.41 m at sunrise, 275.88 m around midday, 255.40 at sunset, and 211.24 m at night. For water bodies, it was 185.32 m, 339.15 m, 282.21 m, and 220.88 m, respectively. Additionally, the CD, CE, and CCE of the water bodies exhibited a gradual increase at night, particularly during the second half of the night. Conversely, the CD, CE, and CCE of the vegetation exhibited a gradual decline. Combined with the results of Kruskal–Wallis analyses (Figure 5), the differences between water bodies and vegetation showed that the CEE was greater for water bodies than for vegetation during the day, while the CEE was greater for vegetation than for water bodies at night. The CD for water bodies was overall greater than vegetation during the day and night. CI, CR, CE, and CS were all significantly greater for water bodies than vegetation during the day, while the difference was not significant at night. This resulted in a gradual increase in the BGCI differences between water bodies and vegetation during the second half of the night.

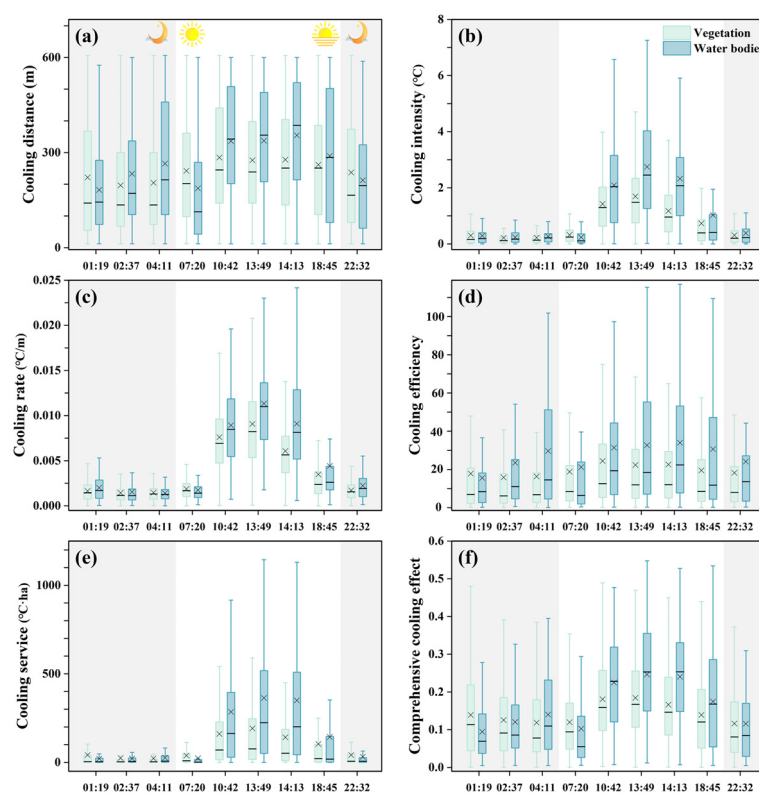


Figure 4. Diurnal variations of BGCI indicators. (a) Cooling distance (CD); (b) cooling intensity (CI); (c) cooling rate (CR); (d) cooling efficiency (CE); (e) cooling service (CS); (f) comprehensive cooling effect (CCE). The light gray background represents night, while the white background represents day. The boxes represent the 25th and 75th percentiles, the horizontal black lines in the boxes represent the median, and the forks represent averages.

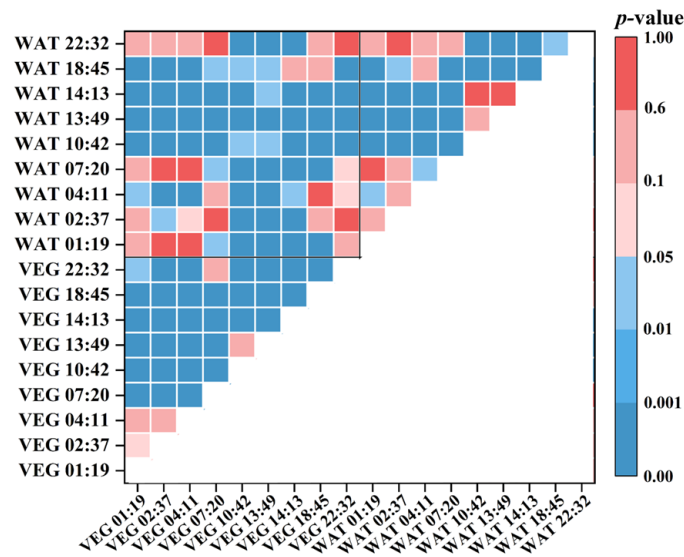


Figure 5. Temporal differences in CCE of vegetation (VEG) and water bodies (WAT). The darker blue represented a greater degree of differentiation, whereas the darker pink represented a greater degree of similarity.

3.2. Overall Impacts of Landscape Metrics on BGCI

In the results of the multiple stepwise regression analyses, the larger the coefficients of determination (R^2) value, the greater the explanatory power of the 2D and 3D landscape metrics on the BGCI indicators. In this study, the total determination coefficient of all landscape metrics on CCE was 0.42, indicating that the 2D and 3D landscape metrics we selected could explain 42% of BGCI changes. Regarding the differences in the BGCI indicators, the R^2 for CS of vegetation was found to be higher than the other indicators (Figure 6), indicating that the landscape metrics had greater explanatory power for the heterogeneity of CS of vegetation. In contrast, the R^2 for water bodies was not found to be significantly different across all BGCI indicators. Moreover, the R^2 value of water bodies (0.57) exceeded that of vegetation (0.26), indicating that the BGCI of vegetation were more susceptible to various factors. The factors influencing the BGCI of vegetation were intricate and could be influenced by factors such as type, configuration structure, and soil composition. The R^2 values for BGCI of vegetation and water bodies exhibited no significant discrepancy between day (0.23, 0.52) and night (0.22, 0.53), although R^2 varied at different times. These findings implied that the overall urban landscape had a comparable impact on the diurnal BGCI of blue-green spaces.

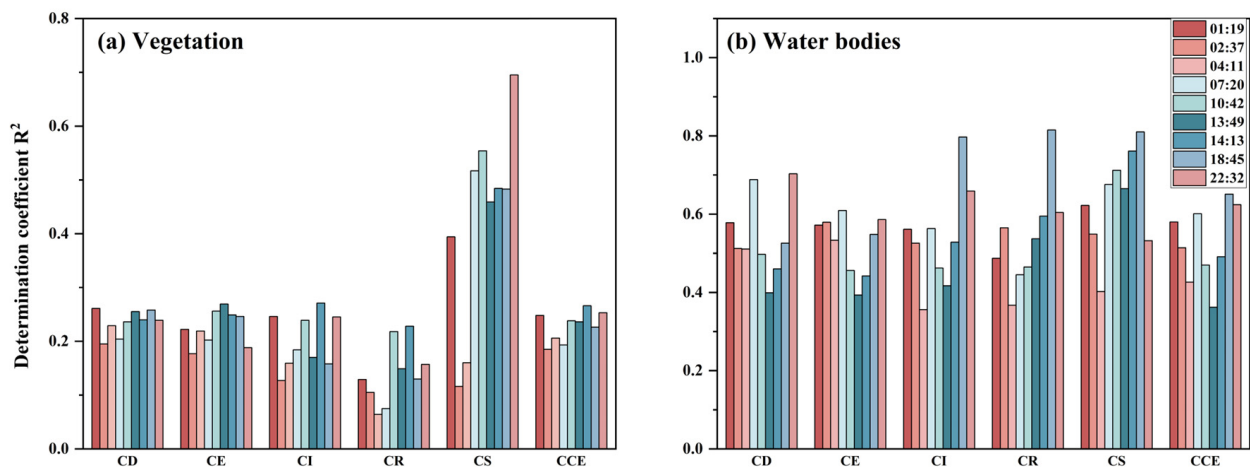


Figure 6. Coefficients of determination of landscape metrics on BGCI indicators at different times.

3.3. Relative Influences and Marginal Effects of 2D and 3D Landscape Metrics

3.3.1. Relative Influences of Landscape Metrics

This study divided the influence factors into six categories and explored the relative influences of each category on the six cooling indicators using the BRT model (Figure 7). The influence factors on the BGCI of blue-green spaces in descending order were 3D metrics (23.82%), Feature (23.51%), Sur_WAT (23.40%), Sur_VEG (13.58%), Sur_ISs (11.03%), and Sur_PEP (4.66%). The dominant factors for most BGCI indicators related to vegetation were 3D metrics and Feature. However, for water bodies, the dominant factors were Sur_WAT, 3D metrics, and Feature.

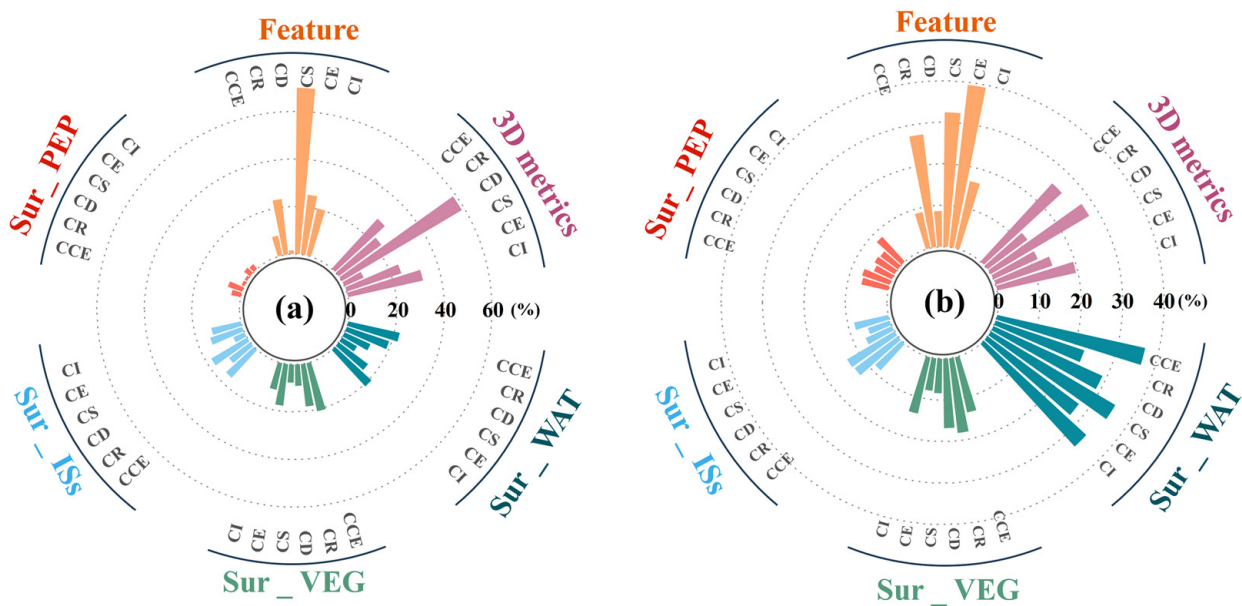


Figure 7. Relative influences of landscape metrics on BGCI indicators throughout the day. (a) Vegetation; (b) water bodies.

There was indeed a diurnal variation in the relative influences on BGCI (Figure 8). During the day, especially around midday, the relative influences of blue-green spaces were distributed similarly. Likewise, the distribution at night also showed some similarity but differed from day patterns. There were variations in the sensitivity of different metrics to different influences. For the CI, CS, and CR of vegetation, the diurnal variation in the composition of influences was more pronounced. Specifically, the relative influences of Feature around midday (32.30%, 80.22%, 44.07%) were more significant compared to night (13.86%, 58.24%, 12.77%), whereas the influences from 3D metrics were more pronounced at night (35.81%, 12.54%, 28.34%) than around midday (26.40%, 5.50%, 16.88%). Diurnal differences in influences on all BGCI metrics in water bodies were significant. Specifically, Features had a significantly higher influence around midday (average 52.87%) than at night (average 10.46%), while Sur_WAT had a higher influence at night (average 38.28%) than around midday (average 15.56%). For CD of water bodies, the influences of 3D metrics were stronger around midday (29.37%) than at night (25.42%). On the contrary, for CI, CE, CS, and CR of water bodies, the influences of 3D metrics were stronger at night (average 20.63%) than around midday (average 9.46%). This indicated that the CD of water bodies is more susceptible to 3D metrics during the day in comparison to other BGCI metrics, as different 3D metrics possess varying ventilation properties. Overall, the Feature of vegetation had a more significant influence on BGCI during the day, while 3D metrics influenced BGCI more at night. Both Feature and 3D metrics of water bodies had a greater influence on BGCI during the day, with Sur_WAT playing a more important role at night.

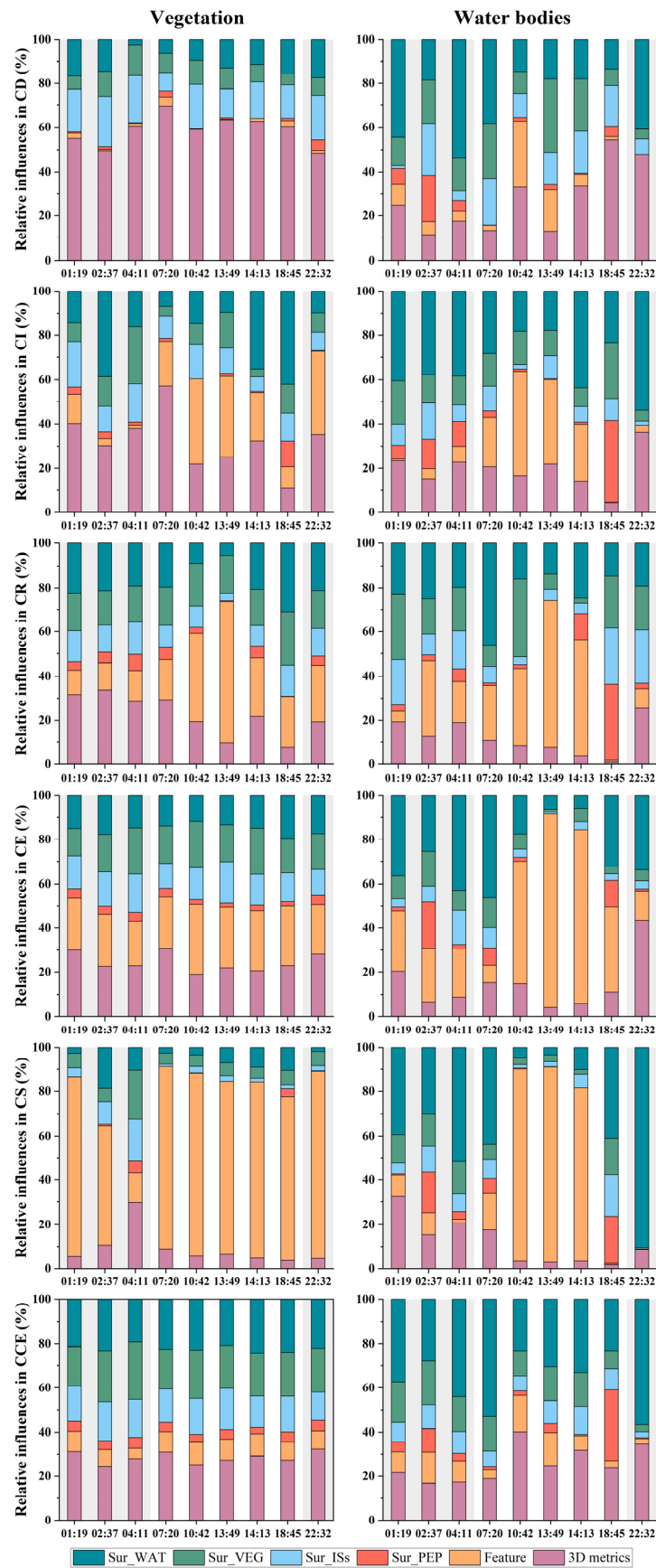


Figure 8. Diurnal variations in the relative influences of 2D and 3D landscape metrics on BGCIs.

3.3.2. Marginal Effects of Dominant Metrics

The marginal effect plot can capture the nonlinear relationship between a single independent variable and the target variable. The slope of the line indicates the strength of this impact. A positive slope indicates a positive correlation between the independent and dependent variables, while a negative slope signifies a negative correlation. In this study, five points in time and six different dominant metrics were selected to analyze the diurnal variation of the marginal effects on CCE of blue-green spaces (Figure 9). The vertical coordinate of the graph was the value of the fitted function of the response variable minus the mean of that function. The marginal effect curves for AREA, Sur_ISs_PLAND of vegetation and AREA, Sur_WAT_NECT, and AHSD of water bodies were steeper around midday, indicating a stronger influence than at night. Conversely, the marginal effect curve of Sur_WAT_NECT of water bodies was steeper at night, indicating a stronger influence than during the day. Moreover, the marginal effect of TH and LSI of vegetation and BCR of water bodies exhibited contrasting trends during midday and at night, displaying significant diurnal variations. In particular, the correlation between the LSI of vegetation and CCE during midday initially declined to approximately three, then rose with an overall upward trend. However, at night, CCE and vegetation LSI were negatively correlated. The marginal benefits of LSI for water bodies presented more intricate results, possibly due to the limited sample size.

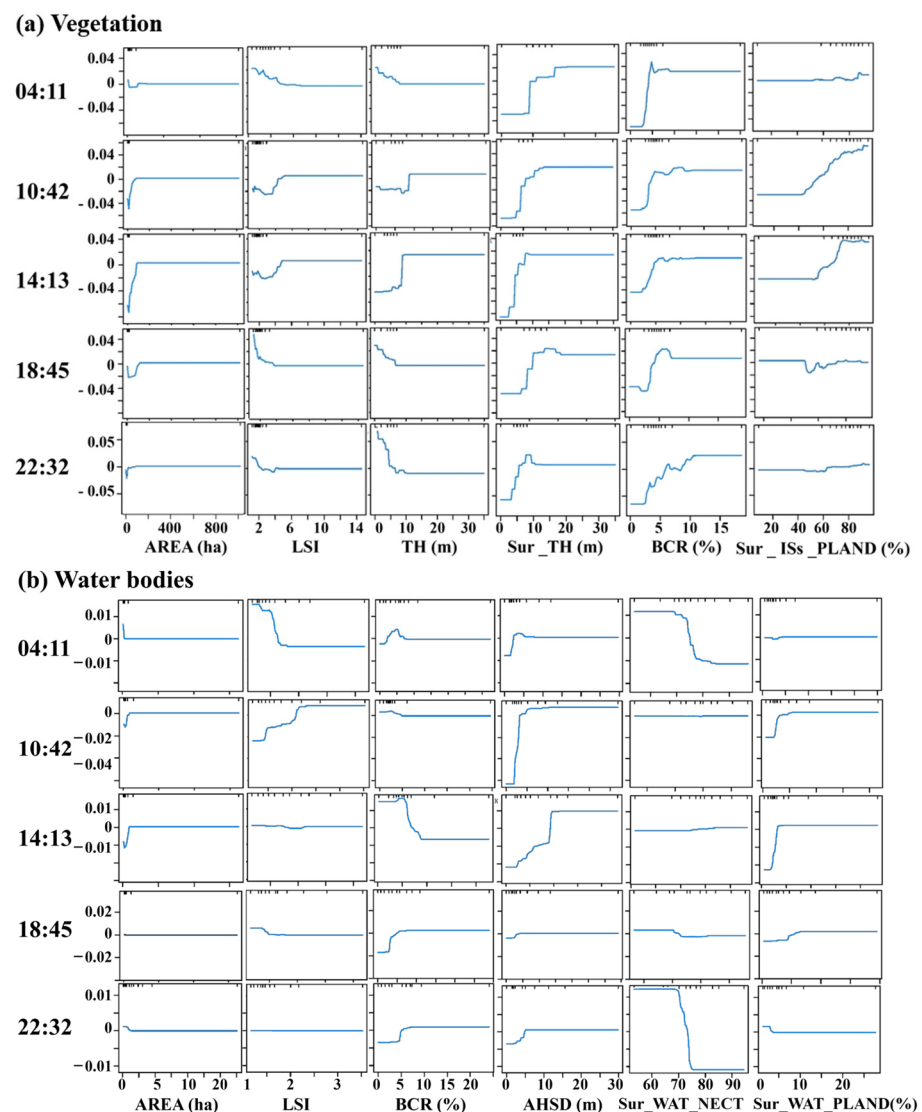


Figure 9. Marginal effects of dominant landscape metrics on CCE.

4. Discussion

4.1. The Temporal Heterogeneity of BGCI

Many previous studies revealed the differences between day and night BGCI effect in blue-green spaces through field investigations and numerical simulations [85–87]. However, few researchers have previously conducted diurnal variations of BGCI at different times of day on a large scale, primarily due to data limitations. Data acquisition from satellites like Landsat and MODIS occurs at specific and single times. The spatial resolution of data from satellites like GOES-R and MSG is not detailed enough to study urban blue-green spaces. This study revealed the diurnal temporal heterogeneity of the BGCI using 70 m ECOSTRESS LST data with flexible acquisition times and found that the BGCI exhibit a distinct pattern of diurnal variations. The BGCI rose steadily from sunrise, peaked around midday, and then declined until sunset, with relatively low and insignificant changes at night. Notably, the BGCI were higher at sunset than at sunrise. The CI was strongest at 13:49, followed by 14:13 and 10:42, with an average difference of 0.5 °C in mean CI. Therefore, there may be some limitations in using Landsat and MODIS data at a single point in time to represent BGCI for urban planning. The LST data obtained from different regions may be from different time points within the diurnal cycle, and the comparison of BGCI using them is also subject to a certain “time error”. Other studies on diurnal variation have also demonstrated varying cooling effects at different time points [29,88].

Vegetation can facilitate cooling through transpiration and the provision of shade [89–91]. The cooling effect of shade is generally consistent with the diurnal variations of solar radiation, with transpiration also occurring at its strongest around midday [92,93]. Furthermore, Wang et al. (2018) found that the contribution of shade to total cooling (60%–75%) is higher than that of transpiration (25%–40%) [94]. Water bodies can evaporate to cool, and evaporation is strongest around midday [95]. Water bodies possess a high specific heat capacity, enabling them to absorb and store heat efficiently, i.e., water bodies per unit mass absorb more heat than ISs to make a change in temperature. In addition, ISs absorb more heat during the day, making the temperature difference between water bodies and ISs greater around midday. The differences in BGCI were related to air temperature [96]. Accordingly, BGCI are most effective around midday, least effective at night, and most effective in the morning and evening. This is consistent with the findings of the field study [97,98]. Wu et al. (2024) also found that the cooling efficiency of vegetation showed a pattern of being strongest at noon and weakest at night [29]. Furthermore, previous studies have indicated that during the daytime, the BGCI of water bodies were greater than vegetation from the LST perspective [28,99]. This study found that the difference in BGCI between water bodies and vegetation was significantly smaller at night than during the day. Additionally, the water bodies did not always exhibit stronger BGCI.

4.2. The Influencing Factors of Diurnal Variation in BGCI

Previous researchers have examined the influencing factors of BGCI at a given time during the day and found that the features of blue-green spaces and the surrounding 2D and 3D urban metrics play important roles [100–102]. Our results showed significant temporal variation in influencing factors, indicating the importance of studying diurnal variations in influencing factors. Zhao et al. (2024) also found that factors influencing LST vary between the daytime and nighttime [103]. The influence of Feature on BGCI was weaker at night than during the day. Wu et al. (2024) suggested that the rise in the relative importance of 3D metrics may be attributed to the increased visibility of tree shadows at 13:38 [29]. Some researchers discovered a negative correlation between the LSI of blue-green spaces and BGCI intensity and efficiency [104–106]. However, other researchers presented the opposite results [107,108]. Yang et al. (2020) discovered that blue-green spaces with a simple LSI were more effective in reducing LST when the area was limited. However, when the area of blue-green spaces exceeds a critical value, blue-green spaces with a complex shape are more effective in reducing summer LST [74]. This study found that BGCI decreased when the LSI of vegetation was slightly more complex around midday. When

the LSI reached the critical value, BGCI were stronger as the LSI was further complicated. However, during sunset and night, BGCI weakened with the complexity of the LSI. In addition, the influence of most of the surrounding 2D metrics on the BGCI of blue-green spaces is more significant at night than during the day.

Previous studies have found that 2D metrics are more closely correlated to LST than 3D metrics [61,109,110]. However, Cao et al. (2021) observed that during the day, 3D metrics exhibited a stronger correlation with the urban environment than 2D metrics [111]. Tian et al. (2019) found that 3D metrics were better than 2D metrics in predicting night and day air temperatures in residential areas [112]. Han et al. (2024) [36] reported that the 3D features exhibited a greater impact on diurnal LST compared with 2D features. Our study found that 3D metrics had the greatest influence on the BGCI of vegetation at night, indicating that 3D metrics highly influenced the process of releasing heat. Wu et al. (2024) also found that the influence of 2D metrics peaked around noon, whereas the influence of 3D metrics peaked at night [29]. This is because a higher aspect ratio of the building and a smaller sky view factor weaken turbulent heat transfer, hindering air circulation and heat release [113–115]. This study also revealed that for vegetation throughout all day and water bodies at night, BCR showed a positive correlation with BGCI. Previous studies concluded that a higher BCR creates more shadows, which favors heat dissipation and thus increases BGCI [60,116–118]. However, this study indicated that this is only one of the reasons, since at night, buildings are unable to create shadows. Another reason for this phenomenon may be that the high BCR results in a large temperature difference between the building and the blue-green spaces, with a consequent increase in sensible heat exchange [119]. However, the relationship between BCR and BGCI in water bodies during the day showed a tendency to increase and then decrease. When the BCR reaches a certain level, it affects the ventilation which in turn affects BGCI. Furthermore, the effect of AHSD on BGCI of water bodies was stronger during the day than at night. Both results indicate that favorable ventilation conditions are more necessary for the BGCI of water bodies during the day. Other studies have also shown that smooth aerodynamics promote health and thermal comfort [120–123]. TH was positively correlated with BGCI during the day, but the opposite is true in the sunset and at night. This opposite phenomenon might be due to the same reason why forests have a warming effect at night [124,125].

4.3. Advantages and Uncertainties

Previous studies on BGCI have mainly focused on a single time point [126,127]. The 70 m spatial resolution and variable observation time provided by ECOSTRESS form the foundation for in-depth analyses of fluctuations in BGCI. Our study results demonstrated the critical importance of monitoring fluctuations in BGCI and the factors that influence them throughout the day. Furthermore, this study quantifies BGCI using five different indicators, and the multi-indicator approach ensures a holistic assessment of the cooling benefits provided by blue-green spaces, making the findings robust and comprehensive.

However, this study has some uncertainties. Firstly, the LST variation in the ECOSTRESS data includes both diurnal and daily variation. Although the nine ECOSTRESS images were acquired on sunny days in the same summer year, they were acquired on different days, which increases the uncertainty in the diurnal variation of the results. Secondly, the use of static population data might not reflect dynamic changes in population density and activity patterns throughout the day, which may lead to uncertainty about the impact of population on the dynamics of BGCI. Subsequently, due to the relatively flat topography of the study area, the study did not consider the effects of wind direction, wind speed, or elevation changes. These unconsidered factors may also contribute to the uncertainty of the results. Furthermore, there are relatively fewer water bodies in the study area. Therefore, there may also be uncertainty in the BGCI for water bodies relative to vegetation.

5. Conclusions

This study explored the diurnal variation of the BGCI in blue-green spaces and the 2D and 3D influence factors within the Fifth Ring Road of Beijing using ECOSTRESS data and the BRT model. The results indicated that BGCI displayed distinct diurnal patterns. BGCI progressively increased from sunrise to midday, decreased thereafter to sunset, reached their peak around midday, and diminished to a relatively low level and constant intensity at night. BGCI of water bodies exhibited a significantly higher intensity compared to vegetation during the day, particularly around midday, while the differences were minimal at night. Moreover, the differences in BGCI between water bodies and vegetation increased gradually during the second half of the night. Using BRT, this study found that the main factors affecting BGCI in blue-green spaces were 3D metrics (23.82%), Features (23.51%), and Sur_WAT (23.40%), followed by Sur_VEG (13.58%) and Sur_ISs (11.03%). The influencing factors also vary considerably at different moments in the diurnal variations. The feature of vegetation had a more significant impact on BGCI during the day, particularly around midday, while the 3D metrics influenced BGCI more at night. Both the features and surrounding 3D metrics of water bodies had a greater impact around midday, with Sur_WAT playing a more important role at night. The effects of Sur_ISs_PLAND of vegetation, Sur_WAT_PLAND, and AHSD of water bodies were significantly greater around midday than at night. Conversely, Sur_WAT_NECT of water bodies had a more pronounced impact at night than around midday. Additionally, the effects of TH, LSI of vegetation, and BCR of water bodies on the BGCI exhibited opposite trends around midday and at night. The effect of Sur_PEP of vegetation and water bodies on CI was significantly greater at 18:45 than at other time points. BGCI cannot simply be considered at a fixed point in time when undertaking urban planning. There is a disparity around midday, but this is not significant in comparison to the morning and evening. Among them, the disparity is strongest at around 13:49. The disparity is even smaller at night, and one point in time during the night can be chosen to represent the whole night.

The findings of this study can provide insights into thermal comfort for urban planning. Regions with high daytime population density, such as roads, can appropriately increase AREA, TH, and LSI; however, regions with high nighttime population density can be left alone for AREA, TH, and LSI. To enhance thermal comfort, it is essential to consider not only the blue-green space itself but also the surrounding landscape, particularly in regions where nighttime thermal comfort is a greater priority. If possible, water bodies can be added around the blue-green space to improve the cooling effect. However, the connectivity of water bodies must be limited in regions with high population density at night.

In regions where there is a greater emphasis on daytime or night-time thermal comfort, it would be beneficial to enhance ventilation in urban areas by reducing BV and increasing AHSD, among other strategies. The exploration of the intraday variations of BGCI and their influencing factors can assist urban planners in creating more scientific urban planning and development management strategies, which could help mitigate the various aspects brought about by the ever-growing UHI effect.

In future studies, we will use ENVI-met to map microclimate variables and set up different scenarios. This will help us assess whether optimizing landscape environments or implementing blue-green spaces with different characteristics can improve urban thermal comfort. Additionally, we aim to demonstrate to policy makers the specific effects and the efficiency of these optimization strategies, including the extent and intensity that can be affected and the changes in impacts over the course of a day.

Author Contributions: Conceptualization, R.K. and Y.C.; methodology, R.K. and H.Z.; software, R.K. and Q.W.; validation, R.K. and Q.W.; formal analysis, Y.H.; investigation, R.K. and C.L.; resources, C.L.; data curation, R.K.; writing—original draft preparation, R.K.; writing—review and editing, Y.C., H.Z., and C.L.; visualization, R.K.; supervision, C.L.; project administration, Y.C. and C.L.; funding acquisition, C.L. All authors have read and agreed to the published version of the manuscript.

Funding: This research was funded by the National Natural Science Foundation of China (Nos. 42471118 and 52308070) and the Youth Innovation Promotion Association of CAS (2021194).

Data Availability Statement: The original contributions presented in the study are included in the article; further inquiries can be directed to the corresponding author.

Acknowledgments: The authors greatly appreciate the assistance of everyone in the Landscape Ecology Group, including Zaiping Xiong, Hongchao Xu, and Jing Zhang.

Conflicts of Interest: The authors declare no conflicts of interest.

References

- Oke, T.R. The Energetic Basis of the Urban Heat Island. *Q. J. R. Meteorolog. Soc.* **1982**, *108*, 1–24. [\[CrossRef\]](#)
- Wang, J.; Chen, Y.; Liao, W.; He, G.; Tett, S.F.B.; Yan, Z.; Zhai, P.; Feng, J.; Ma, W.; Huang, C.; et al. Anthropogenic Emissions and Urbanization Increase Risk of Compound Hot Extremes in Cities. *Nat. Clim. Chang.* **2021**, *11*, 1084–1089. [\[CrossRef\]](#)
- Wang, J.; Chen, Y.; Tett, S.F.B.; Yan, Z.; Zhai, P.; Feng, J.; Xia, J. Anthropogenically-Driven Increases in the Risks of Summertime Compound Hot Extremes. *Nat. Commun.* **2020**, *11*, 528. [\[CrossRef\]](#)
- Singh, N.; Singh, S.; Mall, R.K. Urban Ecology and Human Health: Implications of Urban Heat Island, Air Pollution and Climate Change Nexus. In *Urban Ecology*; Elsevier: Amsterdam, The Netherlands, 2020; pp. 317–334. ISBN 978-0-12-820730-7.
- Ulpiani, G. On the Linkage between Urban Heat Island and Urban Pollution Island: Three-Decade Literature Review towards a Conceptual Framework. *Sci. Total Environ.* **2021**, *751*, 141727. [\[CrossRef\]](#)
- Tian, L.; Lu, J.; Li, Y.; Bu, D.; Liao, Y.; Wang, J. Temporal Characteristics of Urban Heat Island and Its Response to Heat Waves and Energy Consumption in the Mountainous Chongqing, China. *Sustain. Cities Soc.* **2021**, *75*, 103260. [\[CrossRef\]](#)
- Santamouris, M. Recent Progress on Urban Overheating and Heat Island Research. Integrated Assessment of the Energy, Environmental, Vulnerability and Health Impact. Synergies with the Global Climate Change. *Energy Build.* **2020**, *207*, 109482. [\[CrossRef\]](#)
- Chen, B.; Xie, M.; Feng, Q.; Li, Z.; Chu, L.; Liu, Q. Heat Risk of Residents in Different Types of Communities from Urban Heat-Exposed Areas. *Sci. Total Environ.* **2021**, *768*, 145052. [\[CrossRef\]](#)
- Luo, M.; Lau, N. Increasing Human-Perceived Heat Stress Risks Exacerbated by Urbanization in China: A Comparative Study Based on Multiple Metrics. *Earth's Future* **2021**, *9*, e2020EF001848. [\[CrossRef\]](#)
- Raymond, C.; Matthews, T.; Horton, R.M. The Emergence of Heat and Humidity Too Severe for Human Tolerance. *Sci. Adv.* **2020**, *6*, eaaw1838. [\[CrossRef\]](#)
- Zhang, X.; Chen, F.; Chen, Z. Heatwave and Mental Health. *J. Environ. Manag.* **2023**, *332*, 117385. [\[CrossRef\]](#)
- Lo, Y.T.E.; Mitchell, D.M.; Gasparrini, A.; Vicedo-Cabrera, A.M.; Ebi, K.L.; Frumhoff, P.C.; Millar, R.J.; Roberts, W.; Sera, F.; Sparrow, S.; et al. Increasing Mitigation Ambition to Meet the Paris Agreement's Temperature Goal Avoids Substantial Heat-Related Mortality in U.S. Cities. *Sci. Adv.* **2019**, *5*, eaau4373. [\[CrossRef\]](#) [\[PubMed\]](#)
- Cai, W.; Zhang, C.; Zhang, S.; Bai, Y.; Callaghan, M.; Chang, N.; Chen, B.; Chen, H.; Cheng, L.; Cui, X.; et al. The 2022 China Report of the Lancet Countdown on Health and Climate Change: Leveraging Climate Actions for Healthy Ageing. *Lancet Public Health* **2022**, S2468266722002249. [\[CrossRef\]](#)
- Oke, T.R.; Mills, G.; Christen, A.; Voogt, J.A. *Urban Climates*; Cambridge University Press: Cambridge, UK, 2017; ISBN 978-0-521-84950-0.
- Ouyang, Z.; Sciusco, P.; Jiao, T.; Feron, S.; Lei, C.; Li, F.; John, R.; Fan, P.; Li, X.; Williams, C.A.; et al. Albedo Changes Caused by Future Urbanization Contribute to Global Warming. *Nat. Commun.* **2022**, *13*, 3800. [\[CrossRef\]](#)
- Qiao, Z.; Lu, Y.; He, T.; Wu, F.; Xu, X.; Liu, L.; Wang, F.; Sun, Z.; Han, D. Spatial Expansion Paths of Urban Heat Islands in Chinese Cities: Analysis from a Dynamic Topological Perspective for the Improvement of Climate Resilience. *Resour. Conserv. Recycl.* **2023**, *188*, 106680. [\[CrossRef\]](#)
- Shi, Z.; Xu, X.; Jia, G. Urbanization Magnified Nighttime Heat Waves in China. *Geophys. Res. Lett.* **2021**, *48*, e2021GL093603. [\[CrossRef\]](#)
- He, C.; Kim, H.; Hashizume, M.; Lee, W.; Honda, Y.; Kim, S.E.; Kinney, P.L.; Schneider, A.; Zhang, Y.; Zhu, Y.; et al. The Effects of Night-Time Warming on Mortality Burden under Future Climate Change Scenarios: A Modelling Study. *Lancet Planet. Health* **2022**, *6*, e648–e657. [\[CrossRef\]](#)
- Royé, D.; Sera, F.; Tobías, A.; Lowe, R.; Gasparrini, A.; Pascal, M.; de'Donato, F.; Nunes, B.; Teixeira, J.P. Effects of Hot Nights on Mortality in Southern Europe. *Epidemiology* **2021**, *32*, 487–498. [\[CrossRef\]](#)
- Sarangi, C.; Qian, Y.; Li, J.; Leung, L.R.; Chakraborty, T.C.; Liu, Y. Urbanization Amplifies Nighttime Heat Stress on Warmer Days Over the US. *Geophys. Res. Lett.* **2021**, *48*, e2021GL095678. [\[CrossRef\]](#)
- Huang, K.; Lee, X.; Stone, B.; Knievel, J.; Bell, M.L.; Seto, K.C. Persistent Increases in Nighttime Heat Stress from Urban Expansion Despite Heat Island Mitigation. *JGR Atmos.* **2021**, *126*, e2020JD033831. [\[CrossRef\]](#)
- Carvalho, D.; Martins, H.; Marta-Almeida, M.; Rocha, A.; Borrego, C. Urban Resilience to Future Urban Heat Waves under a Climate Change Scenario: A Case Study for Porto Urban Area (Portugal). *Urban Clim.* **2017**, *19*, 1–27. [\[CrossRef\]](#)

23. Venter, Z.S.; Chakraborty, T.; Lee, X. Crowdsourced Air Temperatures Contrast Satellite Measures of the Urban Heat Island and Its Mechanisms. *Sci. Adv.* **2021**, *7*, eabb9569. [[CrossRef](#)] [[PubMed](#)]
24. Bowler, D.E.; Buyung-Ali, L.; Knight, T.M.; Pullin, A.S. Urban Greening to Cool Towns and Cities: A Systematic Review of the Empirical Evidence. *Landsc. Urban Plan.* **2010**, *97*, 147–155. [[CrossRef](#)]
25. Chen, A.; Yao, X.A.; Sun, R.; Chen, L. Effect of Urban Green Patterns on Surface Urban Cool Islands and Its Seasonal Variations. *Urban For. Urban Green.* **2014**, *13*, 646–654. [[CrossRef](#)]
26. Martins, T.A.L.; Adolphe, L.; Bonhomme, M.; Bonneaud, F.; Faraut, S.; Ginestet, S.; Michel, C.; Guyard, W. Impact of Urban Cool Island Measures on Outdoor Climate and Pedestrian Comfort: Simulations for a New District of Toulouse, France. *Sustain. Cities Soc.* **2016**, *26*, 9–26. [[CrossRef](#)]
27. Qian, W.; Li, X. A Cold Island Connectivity and Network Perspective to Mitigate the Urban Heat Island Effect. *Sustain. Cities Soc.* **2023**, *94*, 104525. [[CrossRef](#)]
28. Tan, X.; Sun, X.; Huang, C.; Yuan, Y.; Hou, D. Comparison of Cooling Effect between Green Space and Water Body. *Sustain. Cities Soc.* **2021**, *67*, 102711. [[CrossRef](#)]
29. Wu, W.; Guo, F.; Elze, S.; Knopp, J.; Banzhaf, E. Deciphering the Effects of 2D/3D Urban Morphology on Diurnal Cooling Efficiency of Urban Green Space. *Build. Environ.* **2024**, *266*, 112047. [[CrossRef](#)]
30. Pan, H.; Luo, Y.; Zeng, L.; Shi, Y.; Hang, J.; Zhang, X.; Hua, J.; Zhao, B.; Gu, Z.; Buccolieri, R. Outdoor Thermal Environment Regulation of Urban Green and Blue Infrastructure on Various Types of Pedestrian Walkways. *Atmosphere* **2023**, *14*, 1037. [[CrossRef](#)]
31. Konarska, J.; Holmer, B.; Lindberg, F.; Thorsson, S. Influence of Vegetation and Building Geometry on the Spatial Variations of Air Temperature and Cooling Rates in a High-latitude City. *Int. J. Climatol.* **2016**, *36*, 2379–2395. [[CrossRef](#)]
32. Yan, M.; Chen, L.; Leng, S.; Sun, R. Effects of Local Background Climate on Urban Vegetation Cooling and Humidification: Variations and Thresholds. *Urban For. Urban Green.* **2023**, *80*, 127840. [[CrossRef](#)]
33. Jacobs, S.J.; Gallant, A.J.E.; Tapper, N.J.; Li, D. Use of Cool Roofs and Vegetation to Mitigate Urban Heat and Improve Human Thermal Stress in Melbourne, Australia. *J. Appl. Meteorol. Clim.* **2018**, *57*, 1747–1764. [[CrossRef](#)]
34. Doick, K.J.; Peace, A.; Hutchings, T.R. The Role of One Large Greenspace in Mitigating London’s Nocturnal Urban Heat Island. *Sci. Total Environ.* **2014**, *493*, 662–671. [[CrossRef](#)] [[PubMed](#)]
35. Vaz Monteiro, M.; Doick, K.J.; Handley, P.; Peace, A. The Impact of Greenspace Size on the Extent of Local Nocturnal Air Temperature Cooling in London. *Urban For. Urban Green.* **2016**, *16*, 160–169. [[CrossRef](#)]
36. Qian, F.; Hu, Y.; Wu, R.; Yan, H.; Wang, D.; Xiang, Z.; Zhao, K.; Han, Q.; Shao, F.; Bao, Z. Assessing the Spatial-Temporal Impacts of Underlying Surfaces on 3D Thermal Environment: A Field Study Based on UAV Vertical Measurements. *Build. Environ.* **2024**, *265*, 111985. [[CrossRef](#)]
37. Ossola, A.; Jenerette, G.D.; McGrath, A.; Chow, W.; Hughes, L.; Leishman, M.R. Small Vegetated Patches Greatly Reduce Urban Surface Temperature during a Summer Heatwave in Adelaide, Australia. *Landsc. Urban Plan.* **2021**, *209*, 104046. [[CrossRef](#)]
38. Galalizadeh, S.; Morrison-Saunders, A.; Horwitz, P.; Silberstein, R.; Blake, D. The Cooling Impact of Urban Greening: A Systematic Review of Methodologies and Data Sources. *Urban For. Urban Green.* **2024**, *95*, 128157. [[CrossRef](#)]
39. Chang, Y.; Xiao, J.; Li, X.; Middel, A.; Zhang, Y.; Gu, Z.; Wu, Y.; He, S. Exploring Diurnal Thermal Variations in Urban Local Climate Zones with ECOSTRESS Land Surface Temperature Data. *Remote Sens. Environ.* **2021**, *263*, 112544. [[CrossRef](#)]
40. Hulley, G.; Shivers, S.; Wetherley, E.; Cudd, R. New ECOSTRESS and MODIS Land Surface Temperature Data Reveal Fine-Scale Heat Vulnerability in Cities: A Case Study for Los Angeles County, California. *Remote Sens.* **2019**, *11*, 2136. [[CrossRef](#)]
41. Hulley, G.C.; Göttsche, F.M.; Rivera, G.; Hook, S.J.; Freepartner, R.J.; Martin, M.A.; Cawse-Nicholson, K.; Johnson, W.R. Validation and Quality Assessment of the ECOSTRESS Level-2 Land Surface Temperature and Emissivity Product. *IEEE Trans. Geosci. Remote Sens.* **2022**, *60*, 1–23. [[CrossRef](#)]
42. Ren, Y.; Deng, L.-Y.; Zuo, S.-D.; Song, X.-D.; Liao, Y.-L.; Xu, C.-D.; Chen, Q.; Hua, L.-Z.; Li, Z.-W. Quantifying the Influences of Various Ecological Factors on Land Surface Temperature of Urban Forests. *Environ. Pollut.* **2016**, *216*, 519–529. [[CrossRef](#)] [[PubMed](#)]
43. Nimish, G.; Bharath, H.A.; Lalitha, A. Exploring Temperature Indices by Deriving Relationship between Land Surface Temperature and Urban Landscape. *Remote Sens. Appl. Soc. Environ.* **2020**, *18*, 100299. [[CrossRef](#)]
44. Kowe, P.; Mutanga, O.; Odindi, J.; Dube, T. A Quantitative Framework for Analysing Long Term Spatial Clustering and Vegetation Fragmentation in an Urban Landscape Using Multi-Temporal Landsat Data. *Int. J. Appl. Earth Obs. Geoinf.* **2020**, *88*, 102057. [[CrossRef](#)]
45. Geng, X.; Yu, Z.; Zhang, D.; Li, C.; Yuan, Y.; Wang, X. The Influence of Local Background Climate on the Dominant Factors and Threshold-Size of the Cooling Effect of Urban Parks. *Sci. Total Environ.* **2022**, *823*, 153806. [[CrossRef](#)] [[PubMed](#)]
46. Peng, J.; Liu, Q.; Xu, Z.; Lyu, D.; Du, Y.; Qiao, R.; Wu, J. How to Effectively Mitigate Urban Heat Island Effect? A Perspective of Waterbody Patch Size Threshold. *Landsc. Urban Plan.* **2020**, *202*, 103873. [[CrossRef](#)]
47. Yu, Z.; Guo, X.; Jørgensen, G.; Vejre, H. How Can Urban Green Spaces Be Planned for Climate Adaptation in Subtropical Cities? *Ecol. Indic.* **2017**, *82*, 152–162. [[CrossRef](#)]
48. Fan, H.; Yu, Z.; Yang, G.; Liu, T.Y.; Liu, T.Y.; Hung, C.H.; Vejre, H. How to Cool Hot-Humid (Asian) Cities with Urban Trees? An Optimal Landscape Size Perspective. *Agric. For. Meteorol.* **2019**, *265*, 338–348. [[CrossRef](#)]

49. Cao, X.; Onishi, A.; Chen, J.; Imura, H. Quantifying the Cool Island Intensity of Urban Parks Using ASTER and IKONOS Data. *Landsc. Urban Plan.* **2010**, *96*, 224–231. [[CrossRef](#)]
50. Chen, M.; Jia, W.; Yan, L.; Du, C.; Wang, K. Quantification and Mapping Cooling Effect and Its Accessibility of Urban Parks in an Extreme Heat Event in a Megacity. *J. Clean. Prod.* **2022**, *334*, 130252. [[CrossRef](#)]
51. Xiao, X.D.; Dong, L.; Yan, H.; Yang, N.; Xiong, Y. The Influence of the Spatial Characteristics of Urban Green Space on the Urban Heat Island Effect in Suzhou Industrial Park. *Sustain. Cities Soc.* **2018**, *40*, 428–439. [[CrossRef](#)]
52. Chen, X.; Su, Y.; Li, D.; Huang, G.; Chen, W.; Chen, S. Study on the Cooling Effects of Urban Parks on Surrounding Environments Using Landsat TM Data: A Case Study in Guangzhou, Southern China. *Int. J. Remote Sens.* **2012**, *33*, 5889–5914. [[CrossRef](#)]
53. Sun, R.; Chen, L. How Can Urban Water Bodies Be Designed for Climate Adaptation? *Landsc. Urban Plan.* **2012**, *105*, 27–33. [[CrossRef](#)]
54. Li, X.; Zhou, W. Optimizing Urban Greenspace Spatial Pattern to Mitigate Urban Heat Island Effects: Extending Understanding from Local to the City Scale. *Urban For. Urban Green.* **2019**, *41*, 255–263. [[CrossRef](#)]
55. Qiu, K.; Jia, B. The Roles of Landscape Both inside the Park and the Surroundings in Park Cooling Effect. *Sustain. Cities Soc.* **2020**, *52*, 101864. [[CrossRef](#)]
56. Ruiz, M.A.; Colli, M.F.; Martinez, C.F.; Correa-Cantaloube, E.N. Park Cool Island and Built Environment. A Ten-Year Evaluation in Parque Central, Mendoza-Argentina. *Sustain. Cities Soc.* **2022**, *79*, 103681. [[CrossRef](#)]
57. Du, C.; Jia, W.; Chen, M.; Yan, L.; Wang, K. How Can Urban Parks Be Planned to Maximize Cooling Effect in Hot Extremes? Linking Maximum and Accumulative Perspectives. *J. Environ. Manag.* **2022**, *317*, 115346. [[CrossRef](#)]
58. Liu, Z.; Fu, L.; Wu, C.; Zhang, Z.; Zhang, Z.; Lin, X.; Li, X.; Hu, Y.; Ge, H. Spatialized Importance of Key Factors Affecting Park Cooling Intensity Based on the Park Scale. *Sustain. Cities Soc.* **2023**, *99*, 104952. [[CrossRef](#)]
59. Yang, F.; Yang, D.; Zhang, Y.; Guo, R.; Li, J.; Wang, H. Evaluating the Multi-Seasonal Impacts of Urban Blue-Green Space Combination Models on Cooling and Carbon-Saving Capacities. *Build. Environ.* **2024**, *266*, 112045. [[CrossRef](#)]
60. Han, D.; Xu, X.; Qiao, Z.; Wang, F.; Cai, H.; An, H.; Jia, K.; Liu, Y.; Sun, Z.; Wang, S.; et al. The Roles of Surrounding 2D/3D Landscapes in Park Cooling Effect: Analysis from Extreme Hot and Normal Weather Perspectives. *Build. Environ.* **2023**, *231*, 110053. [[CrossRef](#)]
61. Wu, W.-B.; Yu, Z.-W.; Ma, J.; Zhao, B. Quantifying the Influence of 2D and 3D Urban Morphology on the Thermal Environment across Climatic Zones. *Landsc. Urban Plan.* **2022**, *226*, 104499. [[CrossRef](#)]
62. Xu, H.; Li, C.; Hu, Y.; Li, S.; Kong, R.; Zhang, Z. Quantifying the Effects of 2D/3D Urban Landscape Patterns on Land Surface Temperature: A Perspective from Cities of Different Sizes. *Build. Environ.* **2023**, *233*, 110085. [[CrossRef](#)]
63. Qiao, Z.; Jia, R.; Liu, J.; Gao, H.; Wei, Q. Remote Sensing-Based Analysis of Urban Heat Island Driving Factors: A Local Climate Zone Perspective. *IEEE J. Sel. Top. Appl. Earth Obs. Remote Sens.* **2024**, 1–12. [[CrossRef](#)]
64. Han, D.; An, H.; Wang, F.; Xu, X.; Qiao, Z.; Wang, M.; Sui, X.; Liang, S.; Hou, X.; Cai, H.; et al. Understanding Seasonal Contributions of Urban Morphology to Thermal Environment Based on Boosted Regression Tree Approach. *Build. Environ.* **2022**, *226*, 109770. [[CrossRef](#)]
65. Zhang, Q.; Zhou, D.; Xu, D.; Rogora, A. Correlation between Cooling Effect of Green Space and Surrounding Urban Spatial Form: Evidence from 36 Urban Green Spaces. *Build. Environ.* **2022**, *222*, 109375. [[CrossRef](#)]
66. Jia, S.; Wang, Y.; Liang, T.C.; Weng, Q.; Yoo, C.; Chen, W.; Ding, X. Multiscale Estimation of the Cooling Effect of Urban Greenspace in Subtropical and Tropical Cities. *Urban For. Urban Green.* **2024**, *98*, 128390. [[CrossRef](#)]
67. Li, J.; Wang, H.; Cai, X.; Liu, S.; Lai, W.; Chang, Y.; Qi, J.; Zhu, G.; Zhang, C.; Liu, Y. Quantifying Urban Spatial Morphology Indicators on the Green Areas Cooling Effect: The Case of Changsha, China, a Subtropical City. *Land* **2024**, *13*, 757. [[CrossRef](#)]
68. Cui, Y.; Yan, D.; Hong, T.; Ma, J. Temporal and Spatial Characteristics of the Urban Heat Island in Beijing and the Impact on Building Design and Energy Performance. *Energy* **2017**, *130*, 286–297. [[CrossRef](#)]
69. Qiao, Z.; Chen, J.-Y.; Wang, N.; Lu, Y.-S.; He, T.; Sun, Z.-Y.; Xu, X.-L.; Yang, H.; Li, Y.; Wang, F. Spatial Network of Urban Heat Environment in Beijing-Tianjin-Hebei Urban Agglomeration Based on MSPA and Circuit Theory. *Huan Jing Ke Xue* **2023**, *44*, 3034–3042. [[CrossRef](#)]
70. Song, C.; Yu, Q.; Xing, S.; Wu, Z.; Su, Y.; Ren, Z.; Liu, Y.S. Climate Effects on NDVI Change of Upland Meadow in Dahaituo Nature Reserve over 30 Years. *Acta Ecol. Sin.* **2018**, *38*, 2547–2556. [[CrossRef](#)]
71. Bartesaghi-Koc, C.; Osmond, P.; Peters, A. Mapping and Classifying Green Infrastructure Typologies for Climate-Related Studies Based on Remote Sensing Data. *Urban For. Urban Green.* **2019**, *37*, 154–167. [[CrossRef](#)]
72. Han-qiu, X. A Study on Information Extraction of Water Body with the Modified Normalized Difference Water Index (MNDWI). *Natl. Remote Sens. Bull.* **2005**, *5*, 589–595. [[CrossRef](#)]
73. Li, K.; Li, C.; Liu, M.; Hu, Y.; Wang, H.; Wu, W. Multiscale Analysis of the Effects of Urban Green Infrastructure Landscape Patterns on PM2.5 Concentrations in an Area of Rapid Urbanization. *J. Clean. Prod.* **2021**, *325*, 129324. [[CrossRef](#)]
74. Yang, G.; Yu, Z.; Jørgensen, G.; Vejre, H. How Can Urban Blue-Green Space Be Planned for Climate Adaption in High-Latitude Cities? A Seasonal Perspective. *Sustain. Cities Soc.* **2020**, *53*, 101932. [[CrossRef](#)]
75. Liu, M.; Ma, J.; Zhou, R.; Li, C.; Li, D.; Hu, Y. High-Resolution Mapping of Mainland China's Urban Floor Area. *Landsc. Urban Plan.* **2021**, *214*, 104187. [[CrossRef](#)]

76. Potapov, P.; Li, X.; Hernandez-Serna, A.; Tyukavina, A.; Hansen, M.C.; Kommareddy, A.; Pickens, A.; Turubanova, S.; Tang, H.; Silva, C.E.; et al. Mapping Global Forest Canopy Height through Integration of GEDI and Landsat Data. *Remote Sens. Environ.* **2021**, *253*, 112165. [[CrossRef](#)]
77. Nieves, J.J.; Sorichetta, A.; Linard, C.; Bondarenko, M.; Steele, J.E.; Stevens, F.R.; Gaughan, A.E.; Carioli, A.; Clarke, D.J.; Esch, T.; et al. Annually Modelling Built-Settlements between Remotely-Sensed Observations Using Relative Changes in Subnational Populations and Lights at Night. *Comput. Environ. Urban Syst.* **2020**, *80*, 101444. [[CrossRef](#)] [[PubMed](#)]
78. Peng, J.; Dan, Y.; Qiao, R.; Liu, Y.; Dong, J.; Wu, J. How to quantify the cooling effect of urban parks? linking maximum and accumulation perspectives. *Remote Sens. Environ.* **2021**, *252*, 112135. [[CrossRef](#)]
79. Xiao, Y.; Piao, Y.; Pan, C.; Lee, D.; Zhao, B. Using Buffer Analysis to Determine Urban Park Cooling Intensity: Five Estimation Methods for Nanjing, China. *Sci. Total Environ.* **2023**, *868*, 161463. [[CrossRef](#)] [[PubMed](#)]
80. Yu, Z.; Guo, X.; Zeng, Y.; Koga, M.; Vejre, H. Variations in Land Surface Temperature and Cooling Efficiency of Green Space in Rapid Urbanization: The Case of Fuzhou City, China. *Urban For. Urban Green.* **2018**, *29*, 113–121. [[CrossRef](#)]
81. Qiao, Z.; He, T.; Wang, N.; Wu, F.; Chen, J.; Xu, X.; Liu, L.; Zhang, Q. How Do Natural Factor and Human Activity Affect Urban Land Surface Heat Environment in China? *Ecosyst. Health Sustain.* **2023**, *9*, 0126. [[CrossRef](#)]
82. He, T.; Wang, N.; Tong, Y.; Wu, F.; Xu, X.; Liu, L.; Chen, J.; Lu, Y.; Sun, Z.; Han, D.; et al. Anthropogenic Activities Change Population Heat Exposure Much More than Natural Factors and Land Use Change: An Analysis of 2020–2100 under SSP-RCP Scenarios in Chinese Cities. *Sustain. Cities Soc.* **2023**, *96*, 104699. [[CrossRef](#)]
83. Elith, J.; Leathwick, J.R.; Hastie, T. A Working Guide to Boosted Regression Trees. *J. Anim. Ecol.* **2008**, *77*, 802–813. [[CrossRef](#)] [[PubMed](#)]
84. De'ath, G. Boosted trees for ecological modeling and prediction. *Ecology* **2007**, *88*, 243–251. [[CrossRef](#)] [[PubMed](#)]
85. Shi, D.; Song, J.; Zhong, Q.; Myint, S.W.; Zeng, P.; Che, Y. Cooling Wisdom of 'Water Towns': How Urban River Networks Can Shape City Climate? *Remote Sens. Environ.* **2024**, *300*, 113925. [[CrossRef](#)]
86. Cao, B.; Chen, Q.; Du, M.; Cheng, Q.; Li, Y.; Liu, R. Simulation Analysis of the Cooling Effect of Urban Water Bodies on the Local Thermal Environment. *Water-Sui* **2022**, *14*, 3091. [[CrossRef](#)]
87. Leng, S.; Sun, R.; Yan, M.; Chen, L. Prevalent Underestimation of Tree Cooling Efficiency Attributed to Urban Intrinsic Heterogeneity. *Sustain. Cities Soc.* **2024**, *103*, 105277. [[CrossRef](#)]
88. Liu, Y.; Xu, X.; Wang, F.; Qiao, Z.; An, H.; Han, D.; Luo, J. Exploring the Cooling Effect of Urban Parks Based on the ECOSTRESS Land Surface Temperature. *Front. Ecol. Evol.* **2022**, *10*, 1031517. [[CrossRef](#)]
89. Alkama, R.; Forzieri, G.; Duveiller, G.; Grassi, G.; Liang, S.; Cescatti, A. Vegetation-Based Climate Mitigation in a Warmer and Greener World. *Nat. Commun.* **2022**, *13*, 606. [[CrossRef](#)]
90. Rahman, M.A.; Moser, A.; Rötzer, T.; Pauleit, S. Comparing the Transpirational and Shading Effects of Two Contrasting Urban Tree Species. *Urban Ecosyst* **2019**, *22*, 683–697. [[CrossRef](#)]
91. Rahman, M.A.; Stratopoulos, L.M.F.; Moser-Reischl, A.; Zölch, T.; Häberle, K.-H.; Rötzer, T.; Pretzsch, H.; Pauleit, S. Traits of Trees for Cooling Urban Heat Islands: A Meta-Analysis. *Build. Environ.* **2020**, *170*, 106606. [[CrossRef](#)]
92. Tukiran, J. Cooling Effects of Two Types of Tree Canopy Shape in Penang, Malaysia. *Int. J. Geomate* **2016**, *11*, 2275–2283. [[CrossRef](#)]
93. Bai, Y.; Gaofeng, Z.; Kun, Z.; Ting, M. Research of transpiration and evapotranspiration from a grapevine canopy combining the sap flow and eddy covariance techniques. *Acta Ecol. Sin.* **2015**, *35*, 7821–7831. [[CrossRef](#)]
94. Wang, X.; Kong, F.; Yin, H.; Xu, H.; Li, J.; Pu, Y. Characteristics of Vegetation Shading and Transpiration Cooling Effects during Hot Summer. *Acta Ecol. Sin.* **2018**, *38*, 4234–4244. [[CrossRef](#)]
95. Kang, Z.; Liu, H.; Lu, Y.; Yang, X.; Zhou, X.; An, J.; Yan, D.; Jin, X.; Shi, X. A Novel Approach to Examining the Optimal Use of the Cooling Effect of Water Bodies in Urban Planning. *Build. Environ.* **2023**, *243*, 110673. [[CrossRef](#)]
96. Hathway, E.A.; Sharples, S. The Interaction of Rivers and Urban Form in Mitigating the Urban Heat Island Effect: A UK Case Study. *Build. Environ.* **2012**, *58*, 14–22. [[CrossRef](#)]
97. Du, J.; Jiang, S.; Cui, B.; Wu, G.; Liu, H. Observation-Based Evaluation of Local Climate Effect of Terrestrial Vegetation in Temperate Zones. *JGR Atmos.* **2022**, *127*, e2021JD036313. [[CrossRef](#)]
98. Cruz, J.A.; Blanco, A.C.; Garcia, J.J.; Santos, J.A.; Moscoso, A.D. Evaluation of the Cooling Effect of Green and Blue Spaces on Urban Microclimate through Numerical Simulation: A Case Study of Iloilo River Esplanade, Philippines. *Sustain. Cities Soc.* **2021**, *74*, 103184. [[CrossRef](#)]
99. Xue, Z. Quantifying the Cooling-Effects of Urban and Peri-Urban Wetlands Using Remote Sensing Data: Case Study of Cities of Northeast China. *Landsc. Urban Plan.* **2019**, *182*, 92–100. [[CrossRef](#)]
100. Liao, W.; Guldmann, J.-M.; Hu, L.; Cao, Q.; Gan, D.; Li, X. Linking Urban Park Cool Island Effects to the Landscape Patterns inside and Outside the Park: A Simultaneous Equation Modeling Approach. *Landsc. Urban Plan.* **2023**, *232*, 104681. [[CrossRef](#)]
101. Cai, Z.; Han, G.; Chen, M. Do Water Bodies Play an Important Role in the Relationship between Urban Form and Land Surface Temperature? *Sustain. Cities Soc.* **2018**, *39*, 487–498. [[CrossRef](#)]
102. Yuan, B.; Zhou, L.; Dang, X.; Sun, D.; Hu, F.; Mu, H. Separate and Combined Effects of 3D Building Features and Urban Green Space on Land Surface Temperature. *J. Env. Manag.* **2021**, *295*, 113116. [[CrossRef](#)] [[PubMed](#)]
103. Zhao, K.; Ning, Z.; Xu, C.; Zhao, X.; Huang, X. How Do Driving Factors Affect the Diurnal Variation of Land Surface Temperature across Different Urban Functional Blocks? A Case Study of Xi'an, China. *Sustain. Cities Soc.* **2024**, *114*, 105738. [[CrossRef](#)]

104. Sun, R.; Chen, A.; Chen, L.; Lü, Y. Cooling Effects of Wetlands in an Urban Region: The Case of Beijing. *Ecol. Indic.* **2012**, *20*, 57–64. [[CrossRef](#)]
105. Huang, M.; Cui, P.; He, X. Study of the Cooling Effects of Urban Green Space in Harbin in Terms of Reducing the Heat Island Effect. *Sustainability* **2018**, *10*, 1101. [[CrossRef](#)]
106. Kong, F.; Yin, H.; James, P.; Hutyra, L.R.; He, H.S. Effects of Spatial Pattern of Greenspace on Urban Cooling in a Large Metropolitan Area of Eastern China. *Landsc. Urban Plan.* **2014**, *128*, 35–47. [[CrossRef](#)]
107. Wang, C.; Ren, Z.; Dong, Y.; Zhang, P.; Guo, Y.; Wang, W.; Bao, G. Efficient Cooling of Cities at Global Scale Using Urban Green Space to Mitigate Urban Heat Island Effects in Different Climatic Regions. *Urban For. Urban Green.* **2022**, *74*, 127635. [[CrossRef](#)]
108. Qiu, X.; Kil, S.-H.; Jo, H.-K.; Park, C.; Song, W.; Choi, Y.E. Cooling Effect of Urban Blue and Green Spaces: A Case Study of Changsha, China. *Int. J. Environ. Res. Public Health* **2023**, *20*, 2613. [[CrossRef](#)]
109. Yang, C.; Zhu, W.; Sun, J.; Xu, X.; Wang, R.; Lu, Y.; Zhang, S.; Zhou, W. Assessing the Effects of 2D/3D Urban Morphology on the 3D Urban Thermal Environment by Using Multi-Source Remote Sensing Data and UAV Measurements: A Case Study of the Snow-Climate City of Changchun, China. *J. Clean. Prod.* **2021**, *321*, 128956. [[CrossRef](#)]
110. Huang, X.; Wang, Y. Investigating the Effects of 3D Urban Morphology on the Surface Urban Heat Island Effect in Urban Functional Zones by Using High-Resolution Remote Sensing Data: A Case Study of Wuhan, Central China. *Isprs J. Photogramm. Remote Sens.* **2019**, *152*, 119–131. [[CrossRef](#)]
111. Cao, Q.; Luan, Q.; Liu, Y.; Wang, R. The Effects of 2D and 3D Building Morphology on Urban Environments: A Multi-Scale Analysis in the Beijing Metropolitan Region. *Build. Environ.* **2021**, *192*, 107635. [[CrossRef](#)]
112. Tian, Y.; Zhou, W.; Qian, Y.; Zheng, Z.; Yan, J. The Effect of Urban 2D and 3D Morphology on Air Temperature in Residential Neighborhoods. *Landsc. Ecol.* **2019**, *34*, 1161–1178. [[CrossRef](#)]
113. Kim, J.-J.; Kim, D.-Y. Effects of a Building's Density on Flow in Urban Areas. *Adv. Atmos. Sci.* **2009**, *26*, 45–56. [[CrossRef](#)]
114. Chen, L.; Ng, E.; An, X.; Ren, C.; Lee, M.; Wang, U.; He, Z. Sky View Factor Analysis of Street Canyons and Its Implications for Daytime Intra-urban Air Temperature Differentials in High-rise, High-density Urban Areas of Hong Kong: A GIS-based Simulation Approach. *Int. J. Climatol.* **2012**, *32*, 121–136. [[CrossRef](#)]
115. Yang, J.; Jin, S.; Xiao, X.; Jin, C.; Xia, J.C.; Li, X.; Wang, S. Local Climate Zone Ventilation and Urban Land Surface Temperatures: Towards a Performance-Based and Wind-Sensitive Planning Proposal in Megacities. *Sustain. Cities Soc.* **2019**, *47*, 101487. [[CrossRef](#)]
116. Han, D.; Yang, X.; Cai, H.; Xu, X. Impacts of Neighboring Buildings on the Cold Island Effect of Central Parks: A Case Study of Beijing, China. *Sustainability* **2020**, *12*, 9499. [[CrossRef](#)]
117. Li, H.; Li, Y.; Wang, T.; Wang, Z.; Gao, M.; Shen, H. Quantifying 3D Building Form Effects on Urban Land Surface Temperature and Modeling Seasonal Correlation Patterns. *Build. Environ.* **2021**, *204*, 108132. [[CrossRef](#)]
118. He, B.-J.; Ding, L.; Prasad, D. Wind-Sensitive Urban Planning and Design: Precinct Ventilation Performance and Its Potential for Local Warming Mitigation in an Open Midrise Gridiron Precinct. *J. Build. Eng.* **2020**, *29*, 101145. [[CrossRef](#)]
119. Yu, Z.; Chen, T.; Yang, G.; Sun, R.; Xie, W.; Vejre, H. Quantifying Seasonal and Diurnal Contributions of Urban Landscapes to Heat Energy Dynamics. *Appl. Energy* **2020**, *264*, 114724. [[CrossRef](#)]
120. Murakawa, S.; Sekine, T.; Narita, K.; Nishina, D. Study of the Effects of a River on the Thermal Environment in an Urban Area. *Energy Build.* **1991**, *16*, 993–1001. [[CrossRef](#)]
121. Zhao, L.; Lee, X.; Smith, R.B.; Oleson, K. Strong Contributions of Local Background Climate to Urban Heat Islands. *Nature* **2014**, *511*, 216–219. [[CrossRef](#)]
122. Qiao, Z.; Wang, N.; Chen, J.; He, T.; Xu, X.; Liu, L.; Sun, Z.; Han, D. Urbanization Accelerates Urban Warming by Changing Wind Speed: Evidence from China Based on 2421 Meteorological Stations from 1978 to 2017. *Environ. Impact Assess. Rev.* **2023**, *102*, 107189. [[CrossRef](#)]
123. Niza, I.L.; Bueno, A.M.; Gameiro da Silva, M.; Broday, E.E. Air Quality and Ventilation: Exploring Solutions for Healthy and Sustainable Urban Environments in Times of Climate Change. *Results Eng.* **2024**, *24*, 103157. [[CrossRef](#)]
124. Schultz, N.M.; Lawrence, P.J.; Lee, X. Global Satellite Data Highlights the Diurnal Asymmetry of the Surface Temperature Response to Deforestation. *J. Geophys. Res. Biogeosci.* **2017**, *122*, 903–917. [[CrossRef](#)]
125. Meier, R.; Davin, E.L.; Swenson, S.C.; Lawrence, D.M.; Schwaab, J. Biomass Heat Storage Dampens Diurnal Temperature Variations in Forests. *Environ. Res. Lett.* **2019**, *14*, 084026. [[CrossRef](#)]
126. Yu, Z.; Yang, G.; Zuo, S.; Jørgensen, G.; Koga, M.; Vejre, H. Critical Review on the Cooling Effect of Urban Blue-Green Space: A Threshold-Size Perspective. *Urban For. Urban Gree.* **2020**, *49*, 126630. [[CrossRef](#)]
127. Zhou, W.; Cao, W.; Wu, T.; Zhang, T. The Win-Win Interaction between Integrated Blue and Green Space on Urban Cooling. *Sci. Total Environ.* **2023**, *863*, 160712. [[CrossRef](#)]

Disclaimer/Publisher's Note: The statements, opinions and data contained in all publications are solely those of the individual author(s) and contributor(s) and not of MDPI and/or the editor(s). MDPI and/or the editor(s) disclaim responsibility for any injury to people or property resulting from any ideas, methods, instructions or products referred to in the content.